



LUND UNIVERSITY

Time-lapse electrical resistivity tomography of a water infiltration test on Johannishus Esker, Sweden

Ulusoy, Inan; Dahlin, Torleif; Bergman, Bo

Published in:
Hydrogeology Journal

DOI:
[10.1007/s10040-014-1221-2](https://doi.org/10.1007/s10040-014-1221-2)

2015

[Link to publication](#)

Citation for published version (APA):

Ulusoy, I., Dahlin, T., & Bergman, B. (2015). Time-lapse electrical resistivity tomography of a water infiltration test on Johannishus Esker, Sweden. *Hydrogeology Journal*, 23(3), 551-566. <https://doi.org/10.1007/s10040-014-1221-2>

Total number of authors:
3

General rights

Unless other specific re-use rights are stated the following general rights apply:
Copyright and moral rights for the publications made accessible in the public portal are retained by the authors and/or other copyright owners and it is a condition of accessing publications that users recognise and abide by the legal requirements associated with these rights.

- Users may download and print one copy of any publication from the public portal for the purpose of private study or research.
- You may not further distribute the material or use it for any profit-making activity or commercial gain
- You may freely distribute the URL identifying the publication in the public portal

Read more about Creative commons licenses: <https://creativecommons.org/licenses/>

Take down policy

If you believe that this document breaches copyright please contact us providing details, and we will remove access to the work immediately and investigate your claim.

LUND UNIVERSITY

PO Box 117
221 00 Lund
+46 46-222 00 00



Time-lapse electrical resistivity tomography of a water infiltration test on Johannishus Esker, Sweden

İnan Ulusoy · Torleif Dahlin · Bo Bergman

Abstract Managed aquifer recharge (MAR) is an efficient way to remove organic matter from raw water and, at the same time, reduce temperature variation. Two MAR sites were constructed by Karlskrona municipality on Johannishus Esker in Sweden. One of these sites, Vång, was monitored for electrical conductivity and electrical resistivity (using electrical resistivity tomography - ERT) during a 9-week tracer infiltration test. The aim of the monitoring was to map the pathways of the infiltrated water, with the overall goal to increase the efficiency of the MAR. ERT proved useful in determining both the nature of the esker formation and the water migration pathways. In Vång, the esker ridge follows a tectonically controlled paleo-valley. The fault/fracture zone in the bedrock along this paleo-valley was mapped. During the tracer test, the infiltrated water was detected in the area close to the infiltration ponds, whereas far-situated observation wells were less affected. For sequential infiltration and recharge periods in MAR, the timing of the well pumping is another important factor. Natural groundwater flow direction was a determinant in the infiltration process, as expected. ERT measurements provide supplementary data for site selection, for monitoring the functionality of the MAR sites, and for revealing

the geological, hydrogeological and structural characteristics of the site.

Keywords Artificial recharge · Groundwater management · Sweden · Conductivity · Resistivity change

Introduction

Organic pollution of surface water in areas with high forest coverage and temperate climates is a common problem. Organic matter in drinking water can cause aesthetic and odoriferous problems, as well as increase bacterial growth (Lindroos et al. 2002). If the organic matter content is high, chlorine disinfection can result in the formation of mutagenic or carcinogenic compounds (Lindroos et al. 2002). Organic matter can also interact with pollutants in the soil and groundwater (Thurman 1985; Lindroos et al. 2002), and form compounds and complexes with Fe (Liang et al. 1993; Frycklund and Jacks 1997) and other metals (Nilsson and Bergkvist 1983; Lundström 1993; Lindroos et al. 1995).

An efficient way to remove organic matter from the raw water is managed aquifer recharge (MAR). Using basin infiltration, MAR has been used extensively for decades (e.g. Helmisaari et al. 1998; Frycklund 1998; Lindroos et al. 2002; Greskowiak et al. 2005; Katko et al. 2006; Nöjd et al. 2009). The main idea of MAR is to infiltrate organically polluted water into a structurally well-defined limited area, using the subsurface as a natural filter, and then to produce the water from production wells situated around the infiltration site. The infiltration is made through infiltration basins or ponds, or by sprinkling surface water directly onto the forest floor via a network of pipes (Lindroos et al. 2002). Organic matter is removed from the infiltration water by physical, chemical and microbiological processes in the soil (Lindroos et al. 2002).

Eskers are long, narrow, sinuous, steep-sided ridges composed of irregularly stratified sand and gravel deposited by subglacial or englacial streams flowing between ice walls or in an ice tunnel of a stagnant or retreating glacier and left behind when the ice melted (Flint 1971; Neuendorf et al. 2005). Deposition of an esker happens within or in front of the tunnel mouth (Banerjee and McDonald 1975; Mäkinen 2003; Boulton et al. 2009), within the subglacial (Syverson et al. 1994; Warren and Ashley 1994; Brennand 2000; Campbell 2003; Boulton

Received: 6 May 2014 / Accepted: 5 December 2014
Published online: 24 December 2014

© Springer-Verlag Berlin Heidelberg 2014

Present Address:

İ. Ulusoy
Department of Geological Engineering, Hacettepe University,
06800, Beytepe, Ankara, Turkey

İ. Ulusoy (✉)
Department of Geology, Lund University, Sölvegatan 12,
22362, Lund, Sweden
e-mail: inan@hacettepe.edu.tr
Tel.: +90 312 297 77 00

T. Dahlin
Engineering Geology, Lund University, Box 118, 221 00,
Lund, Sweden

B. Bergman
SWECO Environment, Hans Michelsensgatan 2, Box 286,
201 22, Malmö, Sweden

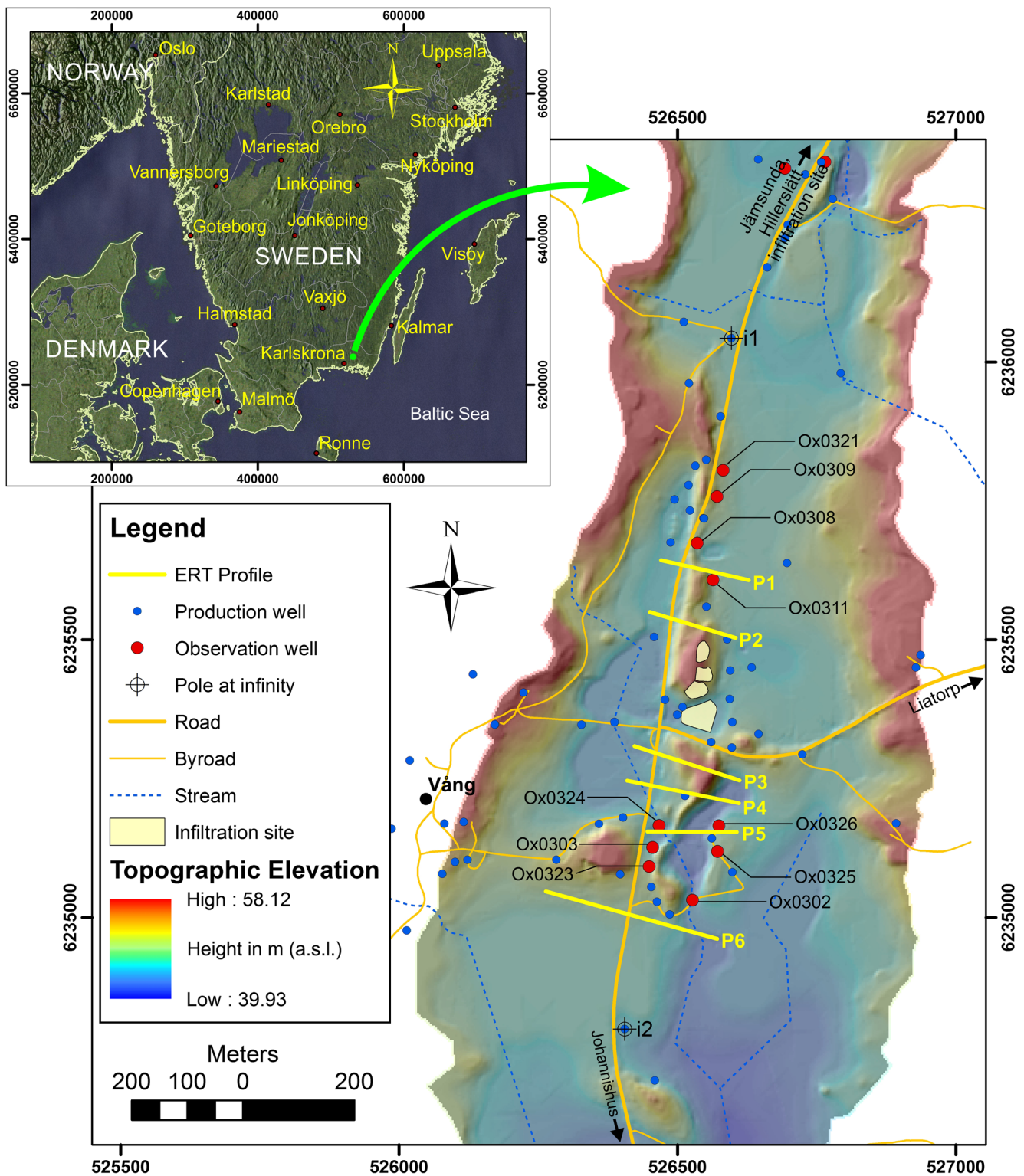


Fig. 1 Map showing the study area. Digital elevation model superimposed on a shaded relief map. Infiltration site, resistivity profiles, and production and observation wells are indicated. Coordinate system: UTM (m), Datum WGS84

et al. 2009) or englacial (Syverson et al. 1994; Campbell 2003; Burke et al. 2009) tunnels, or even in the supraglacial environment (Russell et al. 2001). Eskers have long been known as a natural source of groundwater (De

Geer 1968; Parsons 1970; Artimo et al. 2003; Bolduc et al. 2006; Okkonen et al. 2010), and they are effective sites for MAR (e.g. Lindroos et al. 2002; Katko et al. 2006; Nöjd et al. 2009).

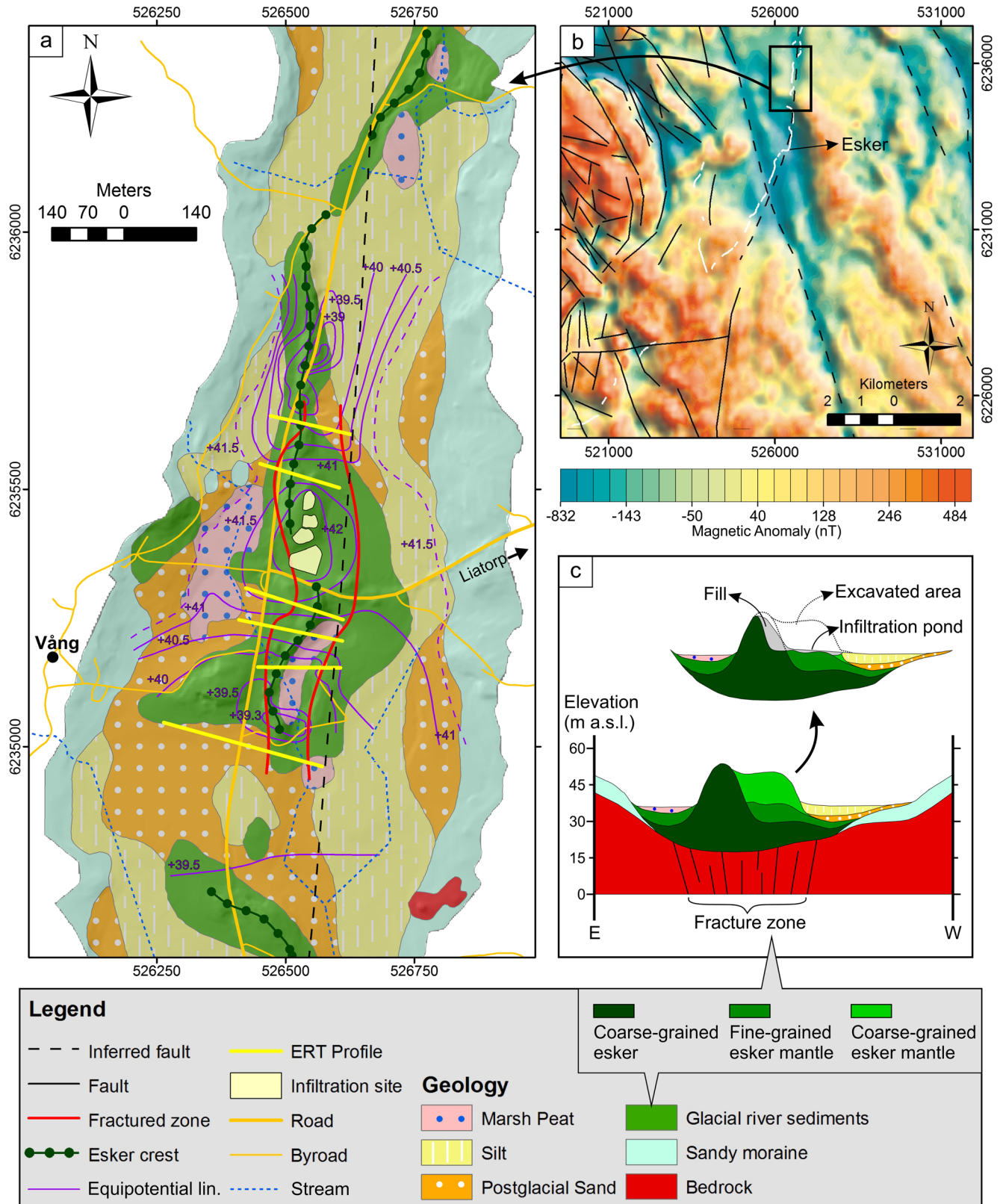


Fig. 2 Geological and structural context of the study area. Coordinate system: UTM (m), Datum WGS84. **a** Geological map (SGU 2012), in which the area *between the red lines* shows the fracture zone revealed by resistivity measurements. Equipotential lines (a.s.l.; Hägg et al. 2010) around the infiltration site interpolated from the data of observation/production wells are shown. **b** Magnetic anomaly map. The map is superimposed on a shaded relief map and shows measured variations in the magnetic total field after subtraction of the geomagnetic reference field (DGRF 1965.0), and is based on airborne measurements performed at an altitude of 30–60 m (SGU 2012). Structural features (see legend) and the Johannishus esker (*white line*) are shown. **c** Simplified geological section of the valley perpendicular to the esker ridge (with changes from Hebrand and Björkman 2005), showing the natural state and the excavated area for infiltration basin construction

Fig. 3 Schedule showing the timeline of the reference and repeated resistivity measurements

Profile	Reference Measurements	Water infiltration	September							October						November	
			Week 1							Week 2	Week 3	Week 4	Week 5	Week 6	Week 7	Week 8	
			21	22	23	24	25	26	27								
P1	✓								✓	✓			✓			✓	
P2	✓								✓	✓	✓		✓				
P3	✓	✓		✓					✓	✓	✓						
P4	✓								✓	✓	✓		✓				
P5	✓								✓	✓	✓		✓				
P6	✓										✓		✓			✓	

Karlskrona Municipality built two MAR facilities on Johannishus Esker (Sweden) for treatment of organically polluted water: the Hillerslätt and Vång infiltration sites. Tracer tests were performed at these MAR sites in 2008. Tests were conducted with salt as a tracer; dosed salt was added to the water and injected through the infiltration ponds. For the Hillerslätt infiltration site in the northern part of the esker, hydraulic connection was shown by the salt recovered in the wells; however, at the southern site, Vång, the rate of recovered tracer in the observation wells remains low when compared to the rate infiltrated. For further investigation of the transport pathways of the infiltrated salty water in the Vång test area, additional tracer experiments were conducted in 2009. New tests were coupled with measurement of electrical conductivity in the observation wells and time-lapse electrical resistivity tomography measurements along six profiles which are detailed and discussed in this report.

Electrical resistivity tomography (ERT) is an efficient technique (Loke and Barker 1996; Barker and Moore 1998) for a wide variety of earth science applications especially in hydrogeology to visualize and monitor the groundwater. Besides aquifer mapping and characterization (Barker and Moore 1998; Dahlin 2001; Corriols and Dahlin 2008; Mendoza et al. 2006), tracer tests can also be monitored with ERT (White 1988, 1994; Morris et al. 1996; Singha and Gorelick 2005; Cassiani et al. 2006).

Geology

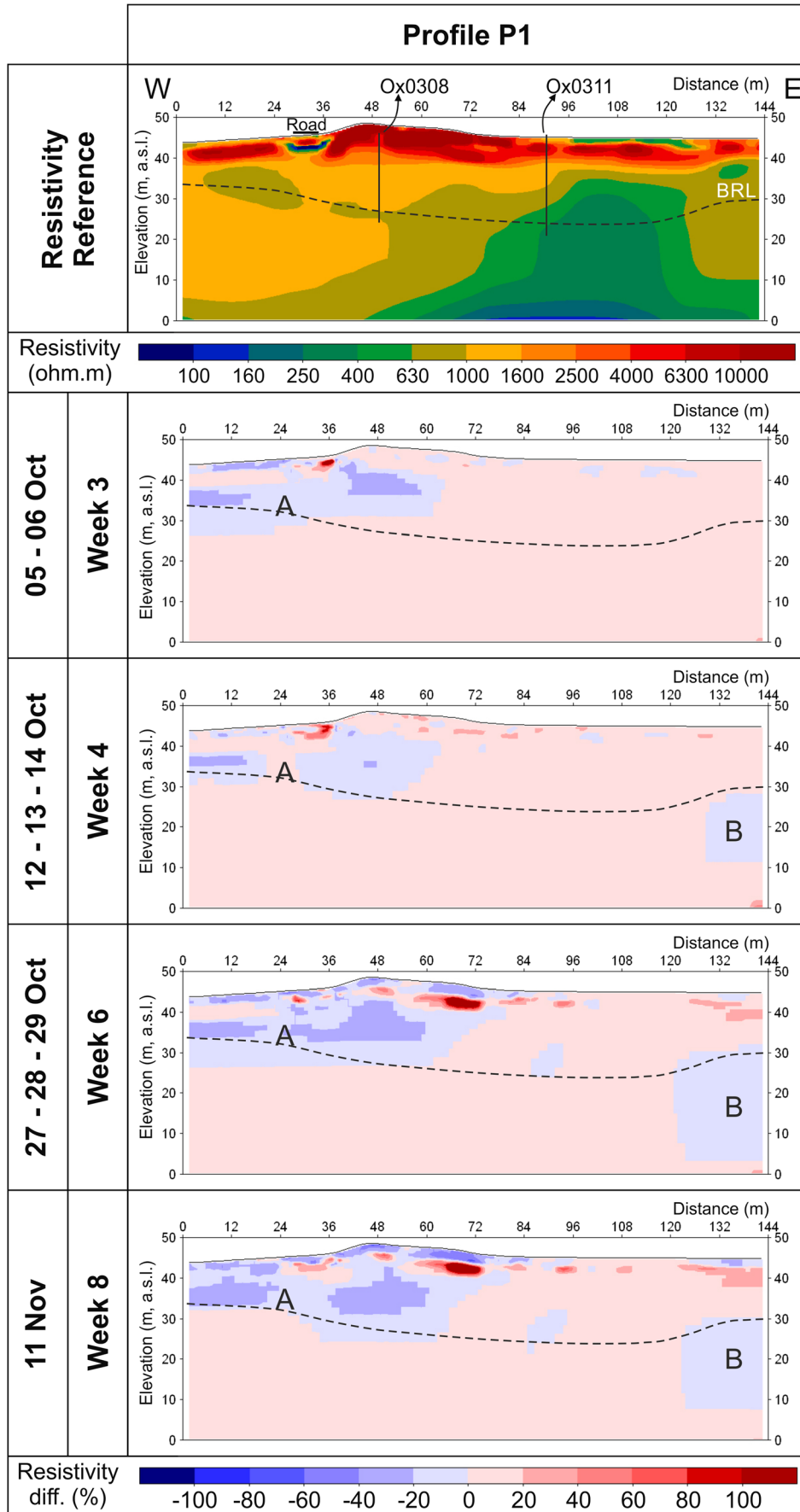
Vång MAR is built on Johannishus Esker near Vång village 4.5 km north of Johannishus and 15 km northwest of Karlskrona (Fig. 1) in Blekinge province. The study area encompasses a NNE-trending valley with a flat, southward sloping morphology and with bounding heights at two edges (western and eastern side) up to 20 m above the valley floor (Fig. 1). Edge to edge, the width of the valley varies from 300 to 900 m. In the middle of the valley, Johannishus Esker is an elongate topographic ridge parallel to the valley direction (Fig. 1).

The geology map of Geological Survey of Sweden (SGU 2012) and a generalized geological section with

changes from Hebrand and Jeppson (1999) and Hebrand and Björkman (2005) are given in Fig. 2a,c. An equipotential contour map (m a.s.l., Hägg et al. 2010) of the infiltration site is projected on Fig. 2a. Johannishus Esker is a NNE trending ridge over 15 km in length (Fig. 2a,b). Near Vång, the crest of the esker reaches 55 m a.s.l. and 12 m above the surrounding flat topography. The width of the esker reaches 130 m in the study area (Fig. 1). The geology is defined by glacial and post-glacial Quaternary sedimentation over mesoproterozoic acidic/intermediate granitic bedrock (SGU 2012, Fig. 2a,c) which is tectonised mainly along N–S fault lines (Berglund et al. 2005; Fig. 2b). Lundqvist and Wohlfarth (2001) state that the coastal area of Blekinge and southeastern Småland up to the highest shoreline became deglaciated ~14,500 years ago. During the deglaciation, Johannishus Esker was deposited in the subaquatic conditions at the margin of the retreating ice-sheet and at the mouth of an ice-tunnel (Malmberg Persson and Persson 2009). As a result, the bedrock is overlaid by sandy moraine and esker deposits, and after the glacial retreat, by post-glacial sand, clay and organic deposits (Fig. 2a,c). Overburden on the bedrock can be up to 30 m within the study area.

The esker deposit can be divided into three main units: the continuous body of the esker deposit and two mantling units above the body (Fig. 2c, Hebrand and Björkman 2005). The body, referred to as coarse-grained esker in Fig. 2c, is the core of the esker deposition, lies on the bedrock and forms the Johannishus ridge. The body consists of well-sorted blocks, gravel and sand, saturated with water and is the most permeable part of the esker (Hebrand and Björkman 2005). Units mantling the esker can be grouped as fine-grained and coarse-grained esker mantle (Fig. 2c, Hebrand and Björkman 2005). Coarse-grained mantle mainly consists of gravel and sand, while fine-grained mantle is mostly stratified fine sand and silt.

Fig. 4 Resistivity profile P1. The reference resistivity profile and the percentage change in resistivity relative to the reference are shown for the repeated measurements. Bedrock level (BRL) is indicated with a dashed line and the relative positions of the closest observation wells are indicated with black lines. Areas marked with A and B represent the resistivity decrease and are discussed in the text



Water infiltration and monitoring methodology

Water infiltration site for MAR

Part of the esker in Vång was previously used as a gravel quarry (Ringberg 1969). It was excavated to depths of 41 m a.s.l. (Fig. 2c) and in the spring of 1979, the excavated area, the hummocky terrain and the remnant esker were levelled out (Hebrand and Björkman 2005). This area was evaluated as an infiltration site by Karlskrona Waterworks (Hebrand 2001); the infiltration ponds were built in the middle portion of the esker crest, close to the Liatorp road (Fig. 1). Two main ponds were constructed: one to the north and one to the south. The southern dam is larger than the northern dam. The topsoil (including the organic horizon and other genetic soil horizons) and fine-grained soil were removed (Fig. 2c), and replaced with coarse-grained pebbles. The constructed infiltration basins have horizontal floors and are 1 m deep with respect to the outer terrain. Infiltration is achieved by sprinkling water over the basin through a suite of parallel pipelines.

A tracer experiment was carried out from September to October 2009 when the natural groundwater level is often at its lowest. Salt infiltration tests were carried out over 6 days by the addition of a total of 15 tonnes of NaCl, which gave a chloride content of 150 mg/L for the water infiltrated. The natural chloride content of the groundwater was 19.1 mg/L (Persson 2008); chloride content at the end of the experiment was 26 mg/L.

Following the infiltration of dosed water, the electrical conductivity of the water in the infiltration dams and in the observation wells (Fig. 1) was logged. Conductivity measurements were carried out by Karlskrona municipality starting just after the infiltration process; data were recorded for 9 weeks.

ERT methodology

In order to trace the infiltration pathways spatially and temporally, repeated resistivity measurements were made along six profiles with fixed electrodes following an initial set of reference resistivity measurements. Reference measurements were carried out in order to get a resistivity image of the area under undisturbed conditions for each profile. The reference data sets were measured when the soils at the surface were very dry, creating some problems in establishing good electrode contact, which to some extent affected the quality of these data. Repeating measurements started in the first week following the initiation of the infiltration test, and during these measurement rounds, electrode contact conditions were more favourable. The first-week measurements were made on the closest profiles, Profiles P2 and P3. Repeated measurements on the remaining lines were completed in the second, third, fourth, sixth and eighth weeks.

Resistivity tests were carried out on six ~E–W oriented profiles (Fig. 1); two profiles are located at the northern side and four of them are at the southern side of the infiltration area. The lengths of profiles P1, P2 and P5 are

160 m, while profiles P3 and P4 are 200 m and profile P6 is 320 m long. Take-out distances of the electrodes are equal (2 m) in all measurements, giving a total electrode spread of 160 m at a single layout. A roll-along procedure (Dahlin 1996) was used to get longer lines with a 160 m spread of four electrode cables. When measurements have been completed on the initial spread, the first cable is shifted to the end of the layout and the new spread is measured; thus, for sections longer than 160 m, the initially installed electrode number is more than 80 electrodes (100 electrodes for 200 m and 160 electrodes for 320 m length). However for the profiles traversing the 8-m-wide road passing by the esker ridge, no electrodes were installed on the road; two to three electrodes were skipped (Fig. 1; profiles P1, P2, P3, P4, and P6). LaBrecque and Daily (2008) showed that iron and steel (and rebar) electrodes produce the smallest errors and create very low noise in resistance and chargeability measurements. Rebar electrodes (~50 cm length) which were installed before the first measurement and retained throughout all the repeated measurements were used. Resistivity measurements were carried out with an ABEM Terrameter SAS4000 resistivity meter integrated with a Lund Imaging System, which is a versatile, multi-channel resistivity system for roll-along profiling (Dahlin 1996, 2001).

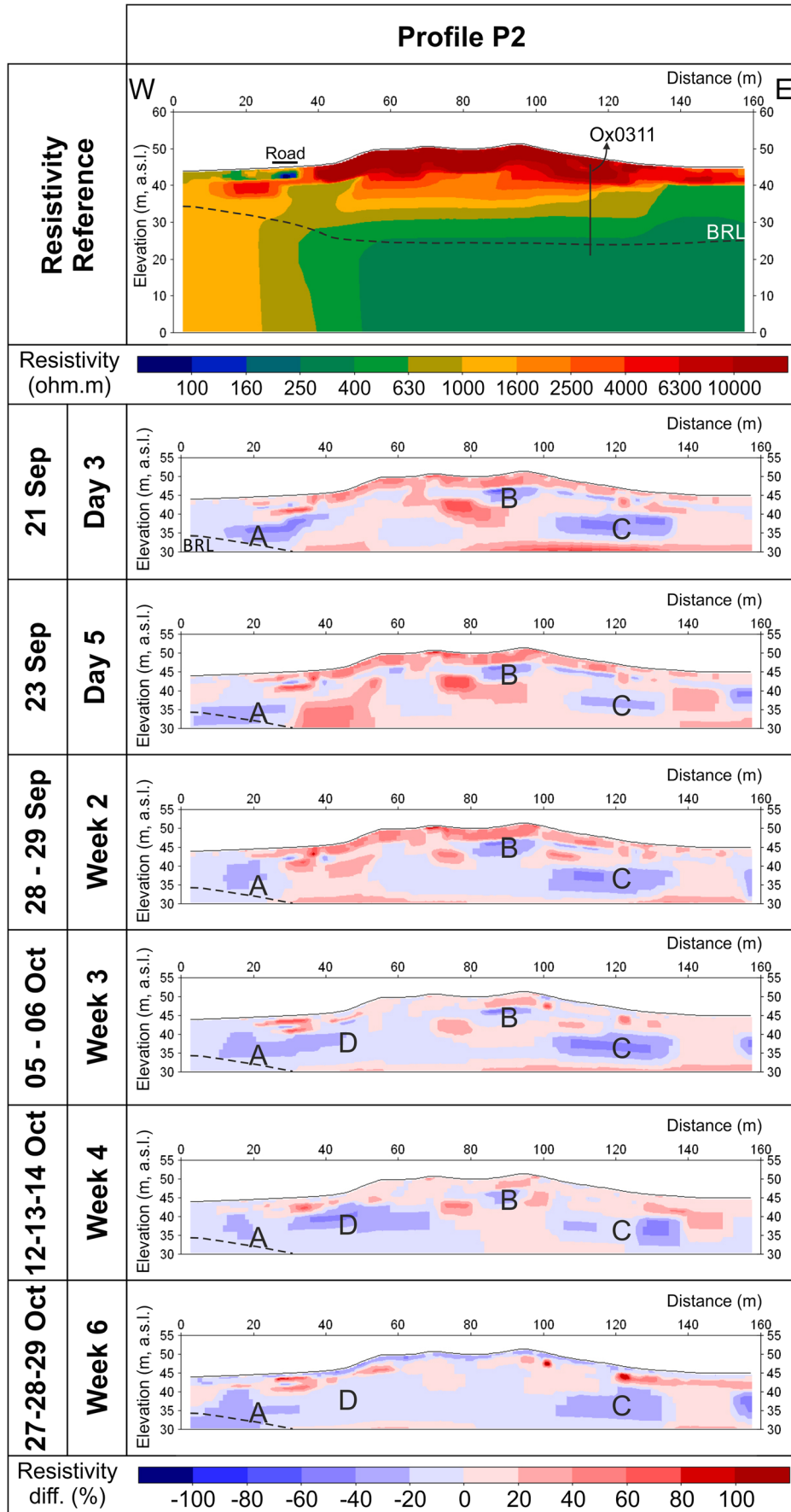
Measurements were made using pole-dipole array, including forward and reverse measurements. The pole at infinity for profiles P1 and P2 was located at 625 m north of the infiltration area (Fig. 1, site i1) and for the rest of the profiles, it was located at 630 m south of the infiltration area (Fig. 1, site i2).

Data processing, interpretation and initial evaluation were done continuously during the experiment. Each repeated resistivity measurement was inverted using time-lapse inversion, and then the percentage difference relative to the inverted reference resistivity model was calculated. Inversion was carried out with Res2DInv using robust (L_1 -norm type) data and model constraint which is better at handling large contrasts in resistivity and noise in data compared to least-squares (L_2 -norm) inversion (Loke et al. 2003). The time-lapse difference (%) calculations and plotting of the inverted sections were made by Erigraph software. Time-lapse datasets were inverted simultaneously using a robust (Claerbout and Muir 1973) smoothness constrain which minimises the absolute changes in the model resistivity values (Loke 1999).

Results

After the reference measurements of all the profiles, and after the start of the infiltration, time-lapse resistivity measurements were conducted. Repetition times for all

Fig. 5 Resistivity profile P2. The reference resistivity profile and the percentage change in resistivity relative to the reference are shown for the repeated measurements. Features are defined as in the caption for Fig. 4. Areas marked with *A*, *B*, *C* and *D* represent the resistivity decrease and are discussed in the text



profiles are summarized in Fig. 3. The initial measurements within the first week were conducted on the two profiles closest to the infiltration area, profiles P2 and P3 (Fig. 1), while the rest of the measurements were made within the following second, third, fourth, sixth, and eighth weeks (Fig. 3). A total of 31 measurements were conducted including the reference measurements. For each repeat measurement, the resistivity change (in percentage) was calculated. The profiles showing the reference resistivity and the percentage change in resistivity are given in Figs. 4, 5, 6, 7 and 8. Bedrock level was observed in 24 of 42 core logs of observation and production wells (between 18.4 and 39.2 m a.s.l.; Hebrand and Björkman 2005; Hägg et al. 2010) and interpreted with resistivity sections. Inferred bedrock levels are plotted in the resistivity sections (Figs. 4, 5, 6, 7 and 8, dashed line, BRL). Relative projections of the closest observation wells are also plotted in the reference resistivity sections (Figs. 4, 5, 6, 7 and 8).

Resistivity signature of Johannishus Esker and surrounding geology

Inverted model resistivities are in the range from <100 ohm.m to >10,000 ohm.m. The esker ridge is represented by high resistivities over ~1,600 ohm.m, which is mostly because of the coarse-grained composition and dry state of the esker. The depth of the high-resistivity signature of the esker extends to 15–25 m (Figs. 4, 5, 6, 7 and 8). Deeper areas in the sections present two distinct resistivity characteristics—first, those with higher resistivities (>1,000 ohm.m), denoting most likely the bedrock at the eastern and western edges of all the profiles; and, second, the low-resistivity areas (<630 ohm.m). These low-resistivity areas were observed at (1) the middle portion of the bedrock just beneath the esker ridge (Figs. 4, 5, 6, 7 and 8), representing most likely the fractured, water-saturated bedrock (Fig. 2c); and (2) above the bedrock along the profile (Figs. 6, 7 and 8), probably representing the younger sedimentation related to fluvio-glacial processes over the bedrock.

Profile P1

Profile P1 is the northernmost profile within the resistivity sections (Fig. 1). Esker sediments are observed with high resistivities (>1,600 ohm.m) at shallow depths (>38 m a.s.l.; Fig. 4). The eastern and western edges of the profile are represented with resistivities between 630 and 1,600 ohm.m. The middle part of the section between ~70 and 120 m horizontally presents low resistivities below 630 ohm.m.

The largest change in resistivity was observed from the western edge to the 80th meter along the profile (Fig. 4, area A). In the third and fourth weeks, a decline in resistivity down to between –20 and –40 % was observed mainly under the esker ridge and at the western edge of the profile. The depth of this negative change extends to 27 m a.s.l. In the third week, shallow depths (~2–3 m from the surface) at the

western edge were also decreasing in resistivity, while the percentage change in resistivity in the fourth week is lower compared to the third week (Fig. 4).

In the sixth and eighth weeks, decrease in resistivity is observed below the esker ridge and in the western part of the esker. The change in the resistivity remained at more than –20 % between depths 30–40 m a.s.l., whereas the decrease at shallow (0–7 m) depths went below –40 % (Fig. 4). In the fourth, sixth and eighth weeks, a very small decline in resistivity (less than –20 %) is indicated at the eastern edge of the profile between 10 and 30 m a.s.l. (Fig. 4, area B).

Profile P2

Profile P2 is one of the two profiles closest to the infiltration site (Fig. 1). Esker sediments stand out with higher resistivities (>1,600 ohm.m) at levels above ~35 m a.s.l. (Fig. 5). Separated with a seemingly vertical transition around 40 m on the profile, the western edge of the profile presents higher resistivities (>630 ohm.m) when compared to the eastern edge (<630 ohm.m) below 30 m a.s.l.

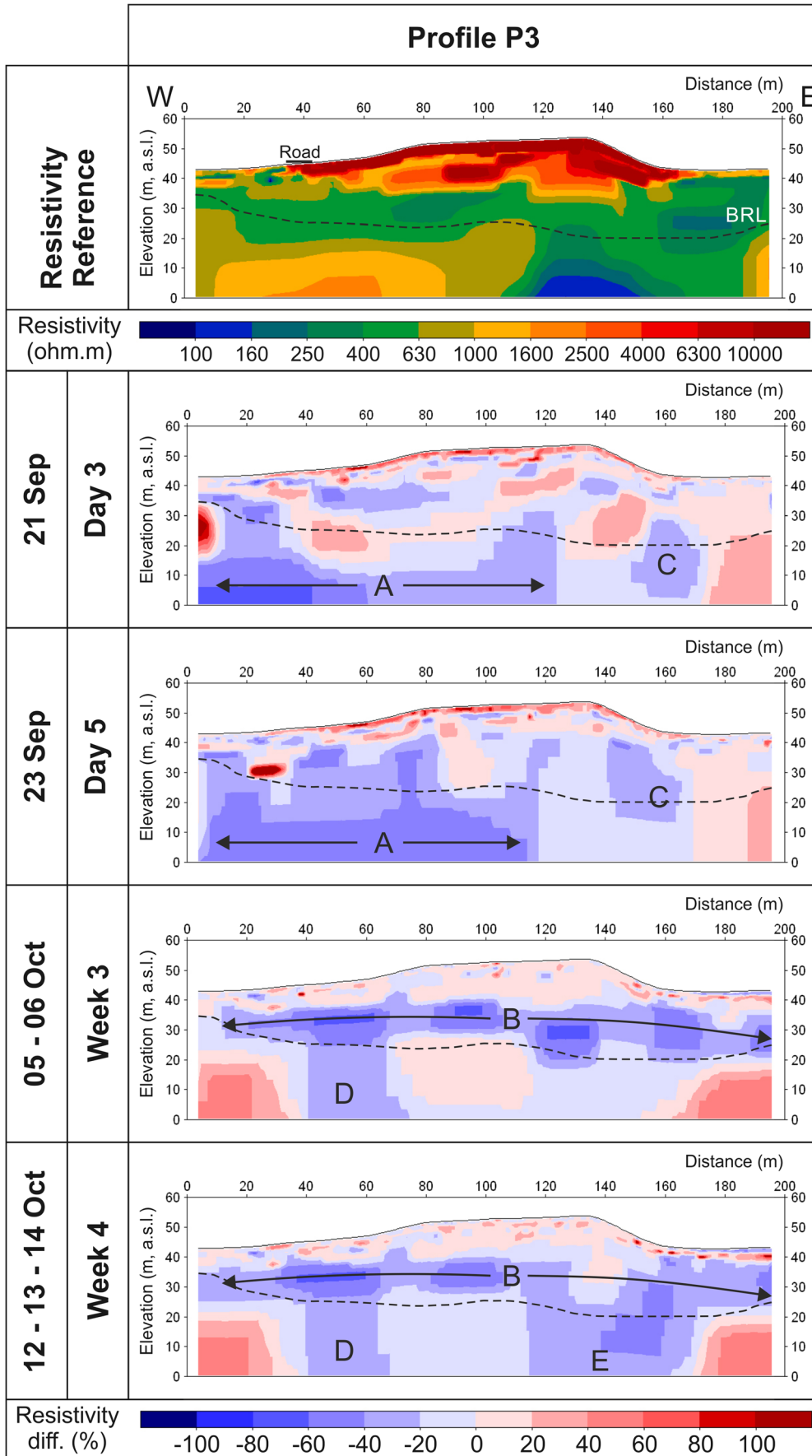
At all the repeated measurements, a negative change (down to below –40 %) in the resistivity was observed below the two sides (Fig. 5, areas A, C) of the esker ridge. Another negative zone ~5 m below the esker ridge disappears in the sixth week (Fig. 5, area B). Starting from the third week, the area indicated with ‘D’ in Fig. 5 presents negative change. This change is in excess of –40 % in the fourth week. As the intensity of the resistivity change decreases, the negatively affected area increases in size throughout time in this profile (Fig. 5). In the shallowest few meters, while the resistivities increase during the first time steps, decrease can be observed following the third week. In the first time steps, increasing resistivities are seen at larger depths in parts of the sections.

Profile P3

Profile P3 is the closest profile to the southernmost infiltration pond (Fig. 1). In the reference resistivity section, the esker ridge appears again with a highly resistive signature (Fig. 6, >1,600 ohm.m). A layer with 160–630 ohm.m resistivities lies along the profile between ~15 and 33 m (a.s.l.), whereas below 20 m (a.s.l.), the western and eastern edges of the profile present high resistivities above 630 ohm.m, and a low-resistivity zone near the eastern side separates them (Fig. 6).

Within the first week of the experiment, a rapid decrease in resistivity is indicated below 20 m a.s.l. at the western side of profile P3, (Fig. 6, area A), while at the

Fig. 6 Resistivity profile P3. The reference resistivity profile and the percentage change in resistivity relative to the reference are shown for the repeated measurements. Features are defined in the caption for Fig. 4. Areas marked with A, B, C, D and E represent the resistivity decrease and are discussed in the text



eastern side, a relatively small decrease is observed (Fig. 6, area C). The area marked with 'A' in Fig. 6 has high resistivity in the reference section. The change in resistivity in this area reaches more than -60 % on the third day. Following the third week, however, there is no more decrease in this area. Rather, the layer marked with 'B' shows a decrease in resistivity (this is the layer represented by 160–630 ohm.m resistivity range in the reference section which overlies the bedrock, Fig. 6). After the third week, relatively lower negative changes occur at the areas indicated by 'D' and 'E'.

In the shallowest few meters, resistivity increase is obvious and most pronounced in the first couple of time

steps. Following the third week, a decrease in the resistivity is observed in the shallow parts of the section.

Profiles P4 and P5

Profiles P4 and P5 are located on the southern edge of the esker ridge (Fig. 1). Reference resistivity sections of profiles P4 and P5 are analogous (Fig. 7) and they also have similarities with profile P3 (Fig. 6). The esker ridge appears as a high resistivity zone (>1,600 ohm.m); at greater depth, the eastern and western edges show resistivities higher than 630 ohm.m and the area in between these edges is represented by low resistivities

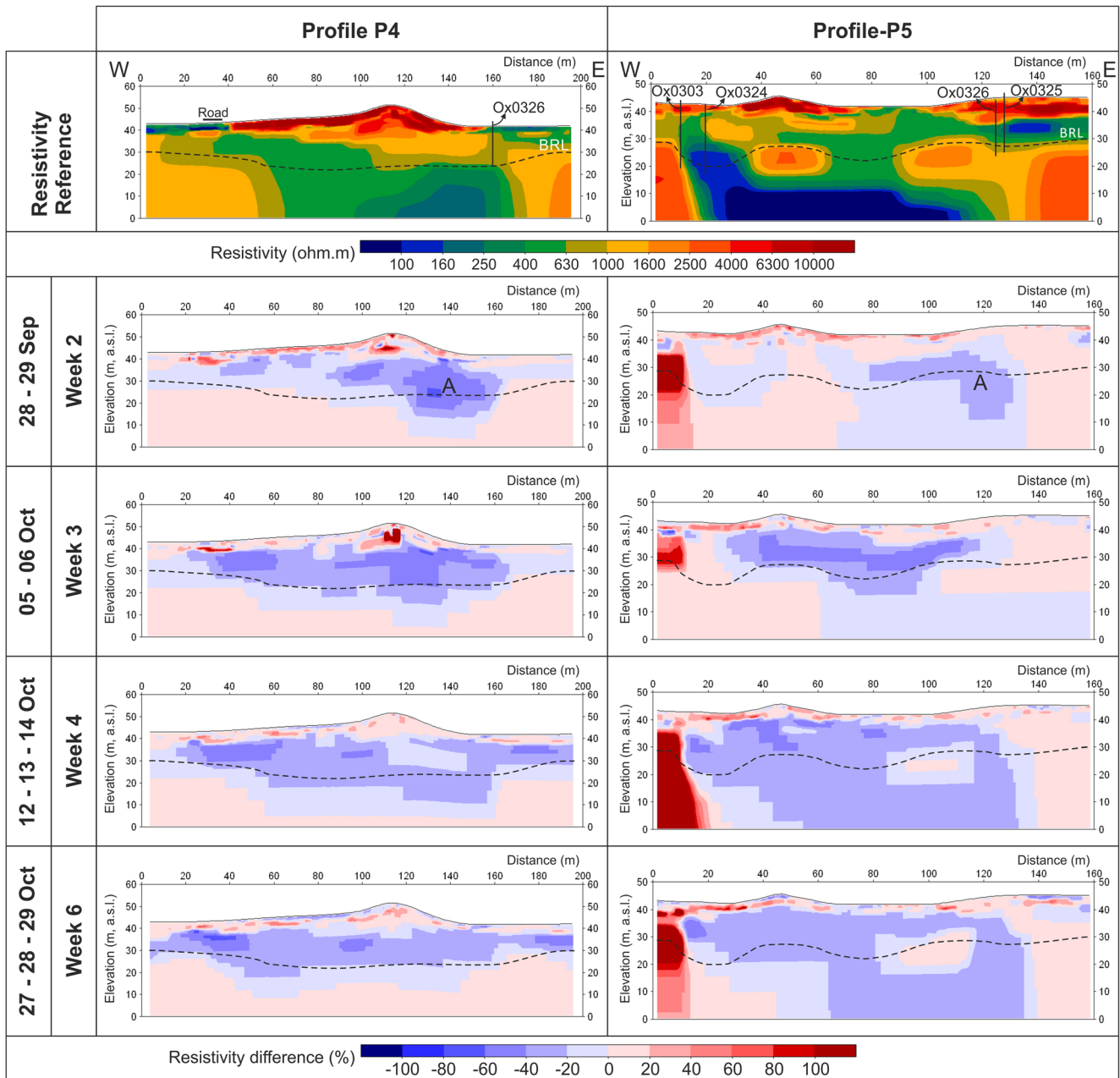


Fig. 7 Resistivity profiles P4 and P5. Reference resistivity profiles and the percentage change in resistivity relative to the reference are shown for the repeated measurements. Features are defined as in the caption for Fig. 4. Area marked with *A* represents the resistivity decrease and is discussed in the text

(<630 ohm.m). In profile P5, two zones defined by high resistivity (630–4,000 ohm.m) are also evident at depth (Fig. 7).

The results for profiles P4 and P5 are clearer than the previous resistivity profiles. In the second week, a decrease in resistivity below -60 and -40 % for profiles P4 and P5, respectively, is evident around the area indicated with 'A' (Fig. 7). This decrease in resistivity spreads through the area under the esker in the third, fourth and sixth weeks, and for the profile P5, deeper infiltration can be interpreted in the fourth and sixth weeks. As with the previous, increasing resistivity is visible in the shallowest part in the first couple of time

steps after the reference, whereas a decrease is seen at the end of the monitoring.

Profile P6

Profile P6 is located just outside of the esker ridge, on the plain surface (Fig. 1). High resistivities corresponding to esker sediments are visible in superficial depths (Figs. 8 and 2). Deeper in the section, high resistivities at the eastern and western edges of the profile suggest bedrock. Similar to profile P3, a layer with lower resistivity lies along the western part of the profile between 10 and 35 m a.s.l. (Fig. 8).

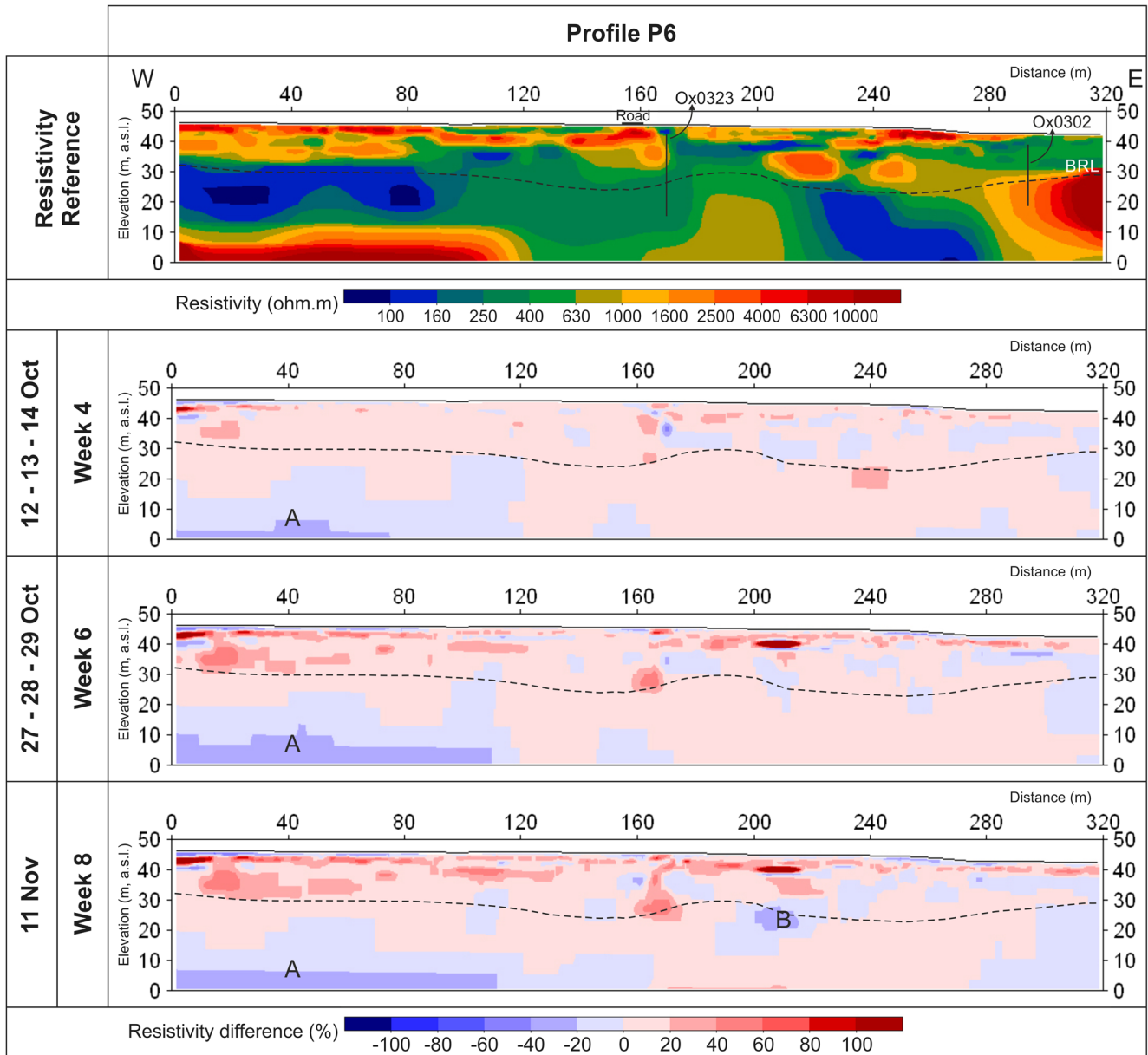


Fig. 8 Resistivity profile P6. Reference resistivity profile and the percentage change in resistivity relative to the reference for the repeated measurements. Features are defined as in the caption for Fig. 4. Areas marked with *A* and *B* represent the resistivity decrease and are discussed in the text

A decrease in the resistivity is barely visible starting from the fourth week and gradually spreading spatially at the end of the eighth week at the western edge of the profile (Fig. 8, area A). The intensity of the change is more than -20% . Another relatively smaller decrease is observed around 25 m a.s.l. (Fig. 8, area B). Zones of increasing resistivity are scattered throughout the relatively shallow parts of the section.

Discussion

Structural control on esker formation

In Finland, Hyypä (1954) and Härme (1961) have related esker trends to fault lines. They proposed that reactivation of old faults, perhaps accompanying isostatic rebound, resulted in lines of weakness in the glacier that then become loci for meltwater flow (Banerjee and McDonald 1975). The majority of the eskers are isolated small ridges that overlie other deposits and follow the underlying topography (Campbell 2003). The majority of the meltwater channels follow existing bedrock/fault-controlled valleys and landscape (Banerjee and McDonald 1975; Shreve 1985; Hebrand and Åmark 1989; Campbell 2003) that form subglacial channels draining meltwater

through the retreating ice. Even in englacial formation of eskers, the importance of structural control is noted by Burke et al. (2009).

Blekinge is a lowland area exposed to a shallow sea, but with a characteristic relief caused by the N–S-trending bedrock ridges (Berglund et al. 2005). Between these ridges there are valleys with fine-grained sediments (Ringberg 1976; Berglund et al. 2005), and glaciofluvial deposits such as eskers and deltas are common in these N–S-trending tectonic valleys (Yu 2003).

Faults and inferred faults coincide with the relative magnetic lows on the magnetic anomaly map of the region (Fig. 2b). The NNE–SSW directed Johannishus Esker is elongated along an inferred fault and along a NNE–SSW-directed negative magnetic anomaly bounded by positive anomalies at eastern and western sides (SGU 2012; Fig. 2b). ERT results show that a corridor of low resistivity elongates through the esker below 30 m a.s.l. (Figs. 4, 5, 6, 7, 8 and 2a, see the area between the red lines). Cored drilling data indicate that this low-resistivity area is the bedrock itself, while the edges of the ERT profiles gave higher resistivities for the bedrock. The reason for the resistivity contrast within the bedrock is most likely because this low-resistivity area is highly fractured, saturated with water and possibly clay weathered, while another possibility

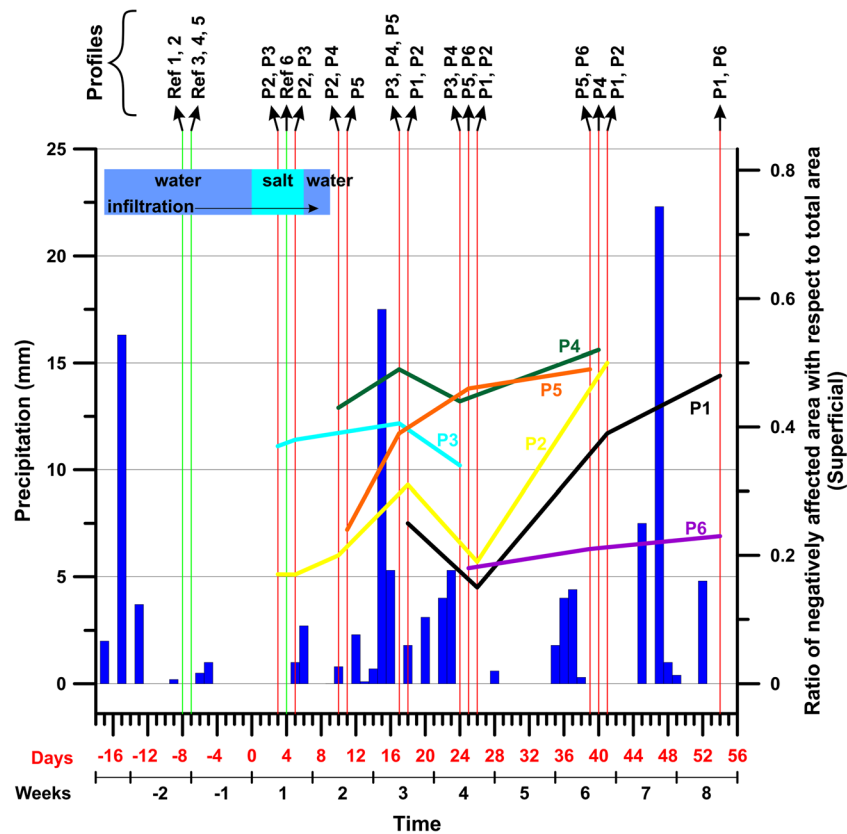
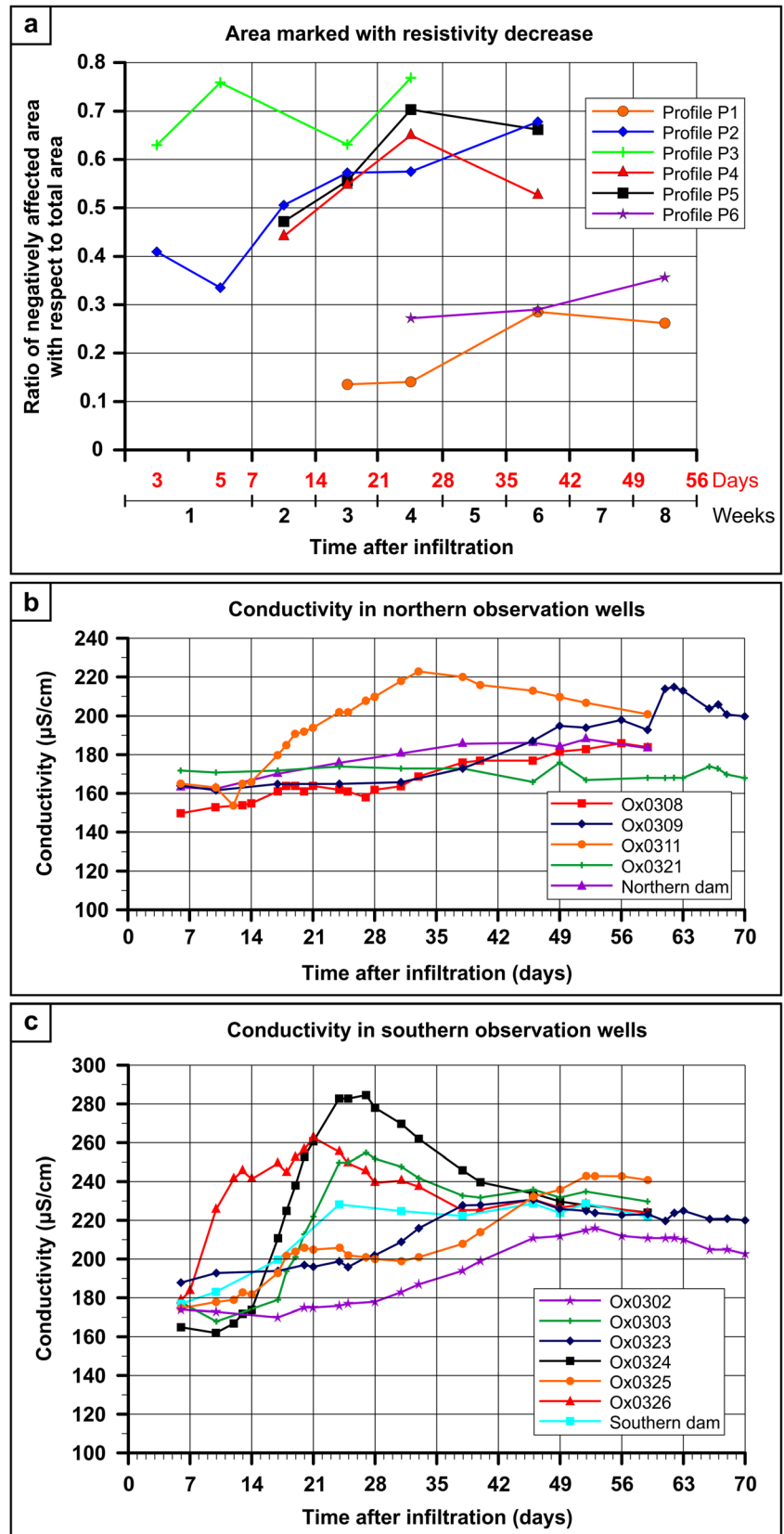


Fig. 9 Change in the ratio of the superficial (top 10 m) negatively affected area with respect to the total area (right vertical scale) throughout the infiltration test with respect to precipitation (left vertical scale). Precipitation data are from Karlshamn station (~36 km from the MAR site) of the Swedish Meteorological and Hydrological Institute

Fig. 10 Change in the affected area and change of electrical conductivity in the observation wells throughout the infiltration test. **a** Area marked with resistivity decrease showing the negatively affected area to total area ratio, **b** Electrical conductivity measured in the northern observation wells, **c** Electrical conductivity measured in the southern observation wells



could be clay infill in the lower parts of the valley. This fracture zone itself is the fault zone, most probably Hydrogeology Journal (2015) 23: 551–566

indicating structural control on the formation of the esker. The paleo-valley controlling the subglacial DOI 10.1007/s10040-014-1221-2

channel that is draining meltwater southward and, thus, forming the esker, was following this fractured zone of the bedrock (Fig. 2c).

Eskers may have been formed on tectonically controlled valleys/zones; thus, it is important to state that for an MAR site, escape of water through the vertical structural features is highly possible. In an unsaturated environment with similar structural conditions, extreme care must be taken to prevent the undesirable loss of water.

Change in resistivity and conductivity during the infiltration test

To visualise and quantify the change in the resistivity, the area showing a decrease in resistivity (negatively affected area) was calculated for each profile. This negatively affected area was calculated both for shallow parts of the sections (top 10 m; Fig. 9) to quantify the superficial change in the resistivity and for the whole sections (Fig. 10a), which implies the infiltration pattern of the salty water. Coloured lines in Figs. 9 and 10a present the 'ratio of the negatively affected area with respect to total/superficial area' versus 'time' for each profile.

The increase in resistivity in the shallow ground is evident in many of the profiles in the early steps of the monitoring period (Figs. 4, 5, 6, 7 and 8). It is almost certainly due to drying out of the shallow ground as it coincided with a very dry period following the summer. The superficial decrease in resistivity that is generally observed in all profiles in the latter weeks similarly was preceded by rain (note the precipitation in Fig. 9).

A decrease in the resistivity was not observed directly at the surface of the esker ridge, but mostly beneath the ridge and in the deeper areas. The elevation of the main infiltration pond (southern dam) is below the ridge (Fig. 1); therefore, the infiltration occurs mostly within the base levels of the esker.

When one focuses on the resistivity change in the whole area of the sections, the largest negatively affected area is observed on the profile P3, which is one of the two profiles closest to the infiltration site (Figs. 10a and 1). The farthest profiles, profile P1 and P6, are the least affected ones. Although profile P6 is almost 200 m away from the infiltration site relative to profile P1, it is affected at least as much as profile P1 (Fig. 10a). A similar phenomenon is observed between profile P2 and profiles P3, P4 and P5. Although the distances of profiles P3 and P2 to the infiltration site are equal (88 m), decrease in resistivity was observed in a larger area in profile P3. In the fourth week, the area showing a decrease in resistivity is larger in profiles P4 and P5 with respect to profile P2. When the distance to the infiltration site is considered, profiles lying south of the infiltration site are affected more than the ones at the northern side (Fig. 10a). This is most likely because the natural groundwater flow direction is from north to south in the valley.

Results of the electrical conductivity measurements for the observation wells situated at the northern and southern

sides of the infiltration site are given in Fig. 10b,c respectively. Two general trends were observed in the conductivity measurements. The first is marked with an almost linearly increasing trend with low slope angle. This is the characteristic trend for the observation wells situated far from the infiltration site (Ox0309, Ox0308, Ox0321, Ox0302, Ox0325, Ox0323; Figs. 1 and 10b,c). Conductivity observed in the northernmost observation well, Ox0321, was almost constant throughout the experiment. The second trend is a rapid increase in conductivity until the fourth and fifth weeks and then a decrease for the rest of the experiment (Fig. 10b,c). This trend was observed in the observation wells close to the infiltration site (Ox0311, Ox0324, Ox0326, Ox0303; Fig. 10b,c) and shows some similarities with the negatively affected area in the resistivity profiles near to them. After a rise in conductivity until the fifth week, conductivity starts to decrease in Ox0311 (Fig. 10b); a similar decrease in the negatively affected area was observed in the closest resistivity profile (profile P1) 1 week later (Fig. 10a). The same relation is observed between the conductivities measured in observation wells Ox0303, Ox0324, Ox0326 (Fig. 10c) and the negatively affected area in profiles P4 and P5 (Fig. 10a), both represented by a decrease starting with the fourth week.

At the western edge of profiles P2, P3 and P6, negative change in the resistivity is first observed in depths associated with the bedrock which is characterized by high resistivity (Figs. 4, 6 and 8). This could be interpreted as infiltration to well-developed fracture/joint systems of the highly resistive bedrock. Another possible explanation could be 3D effects, i.e. the decrease that appears to take place at depth is in fact taking place at shallower depths beside the line. Infiltrated salty water rapidly draining into the fracture/joint systems of the rock may reduce the resistivity of the rock. In profiles P4 and P5, the initial decrease in the resistivity also started in the resistive areas (Fig. 7, area A); in profile P4, decrease was expanded laterally and in profile P5, both laterally and through the deeper areas in the section within the latter weeks (Fig. 7).

On the profiles traversing the road, a bipolar lenticular shaped anomaly was observed beneath the road. The low resistive zones might be associated with application of salt on the road for de-icing purposes; there may also be artefacts due to the skipped electrodes (Figs. 4, 5, 6, 7 and 8). The western edge of profile P5 is located very close to the road, which probably caused the abnormal increase of resistivity in the repeated sections (Figs. 1 and 7).

Conclusion

As inferred from the fault/fracture system mapped by magnetic and ERT measurements, it is evident that the structural control is an important factor in the formation of Johannishus Esker. Pathways of the water during the infiltration test were mapped using ERT. The infiltrated water appears to be concentrated in zones that are the most

rapid pathways for groundwater transport. There is no indication that the infiltrated water escaped through unexpected channels. Infiltrated water largely remained in a limited area relatively close to the infiltration ponds and more distant observation wells were less affected by the infiltrated salty water. ERT and electrical conductivity measurements showed that the infiltrated water affected the down-gradient area more than the up-gradient area relative to the location of the ponds. Natural groundwater flow direction seems to be a determinant factor as expected.

For efficient production of the filtrated water, location of the recharging wells must be selected carefully in relation to the preferential pathways for groundwater transport. For example, profiles P3, P4 and P5 reveal locations that may be optimal for production wells from that point of view. Transport time is also important for effective recharge, on one hand to be able to recharge sufficient amounts of water, but on the other hand to have sufficient time in transit to achieve the desired cleaning effect. Conductivity monitoring and water infiltrated areas mapped with ERT show that the highest concentration time was around 4–5 weeks with the tested production rate (Fig. 10). This result was supported both by the conductivity and ERT measurements (Fig. 10).

The efficiency of the MAR sites may vary according to the geological, structural and hydrogeological conditions of the site. Efficiency in terms of the rate of infiltrated and recharged water does not promote good quality of the filtrated water. Water quality is also another important factor in determining the location of the production wells. ERT measurements before the site selection and ERT monitoring during the initial stage of the functionality of the MAR sites may reveal important information for further planning for efficient production.

Acknowledgements This work was funded by Karlskrona Municipality, Sweden, whom we thank for permission to publish the results. The field test and evaluation of the results, from a design and production point of view, was carried out by Sweco VIAK, Malmö, Sweden. Inan Ulusoy was guest researcher at Lund University thanks to a grant from the Swedish Institute, which is gratefully acknowledged. The authors are grateful to P. Comida for supporting the field activity. We are very grateful to Dr. Alfredo Mendoza and Dr. Mats Hebrand for their astute comments and constructive remarks on the earlier draft of the manuscript, and Jan Lindberg for help with documentation from the field test. We are thankful to Dr. Richard Owen for his constructive remarks and for improving the English of the manuscript. Furthermore, we wish to thank Jacopo Boaga and two anonymous reviewers for constructive criticism on the manuscript.

References

- Artimo A, Mäkinen J, Berg RC, Abert CC, Salonen V-P (2003) Three-dimensional geologic modeling and visualization of the Virtaankangas aquifer, southwestern Finland. *Hydrogeol J* 11:378–386
- Banerjee I, McDonald BC (1975) Nature of esker sedimentation. *Glaciofluvial Glaciolacustrine Sedimentol* 23:132–154
- Hydrogeology Journal (2015) 23: 551–566
- Barker RD, Moore J (1998) The application of time-lapse electrical tomography in groundwater studies. *Lead Edge* 17:1454–1458
- Berglund BE, Sandgren P, Barnekow L, Hannon G, Jiang H, Skog G, Yu S-Y (2005) Early Holocene history of the Baltic Sea, as reflected in coastal sediments in Blekinge, southeastern Sweden. *Quat Int* 130:111–139
- Bolduc A, Paradis SJ, Riverin M-N, Lefebvre R, Michaud Y (2006) A 3D Esker geomodel for groundwater research: the case of the Saint-Mathieu-Berry esker, Abitibi, Québec, Canada. In: Russell HAJ, Berg RC, Thorleifson HL (eds) 3D geologic mapping for groundwater applications: workshop extended abstracts. *Geol Surv of Can Open File* 5048
- Boulton GS, Hagdorn M, Maillot PB, Zatsepin S (2009) Drainage beneath ice sheets: groundwater–channel coupling, and the origin of esker systems from former ice sheets. *Quat Sci Rev* 28:621–638
- Brennand TA (2000) Deglacial meltwater drainage and glaciodynamics: inference from Laurentide eskers, Canada. *Geomorphol* 32:263–293
- Burke MJ, Woodward J, Russell AJ, Fleisher PJ (2009) Structural controls on englacial esker sedimentation: Skeiðarárjökull, Iceland. *Ann Glaciol* 50(51):85–92
- Campbell JE (2003) Quaternary investigations in the Patterson Island area (part of NTS 64E-10 and -15), Reindeer Lake, Eastern Peter Lake Domain. In: Summary of Investigations 2003, vol 2. Misc. Rep. 2003-4.2, Paper A-7, Saskatchewan Geological Survey, Sask. Industry Resources, Regina, SK, 16 pp
- Cassiani G, Bruno V, Villa A, Fusi N, Binley AM (2006) A saline trace test monitored via time-lapse surface electrical resistivity tomography. *J Appl Geophys* 59(3):244–259
- Claerhout JF, Muir F (1973) Robust modeling with erratic data. *Geophys* 38:826–844
- Corriols M, Dahlin T (2008) Geophysical characterization of the León-Chinandega aquifer, Nicaragua. *Hydrogeol J* 16:349–362
- Dahlin T (1996) 2D resistivity surveying for environmental and engineering applications. *First Break* 14(7):275–283
- Dahlin T (2001) The development of DC resistivity imaging techniques. *Comput Geosci* 27:1019–1029
- de Geer J (1968) Some hydrogeological aspects on aquifers, especially eskers. In: Eriksson E, Gustafsson Y, Nilsson K (eds) *Groundwater problems*. Pergamon, New York
- Flint RF (1971) *Glacial and Quaternary geology*. Wiley, New York
- Frycklund C (1998) Long-term sustainability in artificial groundwater recharge. In: Peters JH et al (eds) *Artificial recharge of groundwater*. Balkema, Rotterdam
- Frycklund C, Jacks G (1997) Iron and artificial recharge of groundwater. *Boreal Environ Res* 2:171–81
- Greskowiak J, Prommer H, Massmann G, Johnston CD, Nützmann G, Pekdeger A (2005) The impact of variably saturated conditions on hydrogeochemical changes during artificial recharge of groundwater. *Appl Geochem* 20:1409–1426
- Hägg M, Bergman B, Lindberg J, Hebrand M (2010) Karlskrona Kommun, Karlskrona vatten: fullskaleförsök med saltinfiltration och geofysiska mätningar [Karlskrona municipality, Karlskrona water: full scale tests with salt infiltration and geophysical surveys]. SWECO VBB VIAK 1240121000, Sweco, Malmö, Sweden, 56 pp
- Härme M (1961) On the fault lines in Finland. *Bull Comm Geol Finlande* 196:437–444
- Hebrand M (2001) Karlskrona municipality, Karlskrona water: technical description of water activity at Johannishus ridge (in Swedish). VBB VIAK 1240121, Malmö, Sweden, 48 pp
- Hebrand M, Åmark M (1989) Esker formation and glacier dynamics in eastern Skåne and adjacent areas, southern Sweden. *Boreas* 18:67–81
- Hebrand M, Björkman F (2005) Karlskrona vattenförsörjning: undersökning av infiltrationsområden vid Johannishusåsen [Karlskrona water supply: investigation of infiltration areas at Johannishus Ridge]. SWECO VIAK 1240121, Sweco, Malmö, Sweden, 59 pp

- Hebrand M, Jeppson H (1999) Karlskrona municipality, Karlskrona water: hydrogeological investigations at Johannishus Ridge 1997–1999 (in Swedish). SWECO VBB VIAK 1240121, Malmö, Sweco, Sweden, 130 pp
- Helmisaari H-S, Kitunen V, Lindroos A-J, Lumme I, Monni S, Nöjd P, Paavolainen L, Pesonen E, Salemaa M, Smolander A, Derome J (1998) Sprinkling infiltration in Finland: effects on forest soil, percolation water and vegetation. In: Peters JH et al (eds) Artificial recharge of groundwater. Balkema, Rotterdam
- Hyypä E (1954) Åsarnas uppkomst [Genesis of ridges]. *Geolog* 6:45
- Katko TS, Lipponen MA, Rönkä EKT (2006) Groundwater use and policy in community water supply in Finland. *Hydrogeol J* 14:69–78
- LaBrecque D, Daily W (2008) Assessment of measurement errors for galvanic-resistivity electrodes of different composition. *Geophysics* 73(2):F55–F64
- Liang L, McCarthy JF, Jolley LW, McNabb JA, Mehlhorn TL (1993) Iron dynamics: transformation of Fe(II)/Fe(III) during injection of natural organic matter in a sandy aquifer. *Geochim Cosmochim Acta* 57:1987–1999
- Lindroos A-J, Derome J, Niska K (1995) The relationship between dissolved organic matter and percolation water chemistry in northern Finland. *Water Air Soil Pollut* 79:191–200
- Lindroos A-J, Kitunen V, Derome J, Helmisaari H-S (2002) Changes in dissolved organic carbon during artificial recharge of groundwater in a forested esker in southern Finland. *Water Res* 36:4951–4958
- Loke MH (1999) Time-lapse resistivity imaging inversion. Proceedings of the 5th Meeting of the Environmental and Engineering Geophysical Society European Section, Em 1, Budapest, September 1999
- Loke MH, Barker RD (1996) Rapid least squares inversion of apparent resistivity pseudosections by a quasi-Newton method. *Geophys Prospect* 44:131–152
- Loke MH, Acworth I, Dahlin T (2003) A comparison of smooth and blocky inversion methods in 2-D electrical imaging surveys. *Explor Geophys* 34(3):182–187
- Lundqvist J, Wohlfarth B (2001) Timing and east–west correlation of south Swedish ice marginal lines during the Late Weichselian. *Quat Sci Rev* 20:1127–1148
- Lundström US (1993) The role of organic acids in the soil solution chemistry of a podzolized soil. *J Soil Sci* 44:121–133
- Mäkinen J (2003) Time-transgressive deposits of repeated depositional sequences within interlobate glaciofluvial (esker) sediments in Köyliö, SW Finland. *Sedimentology* 50:327–360
- Malmberg Persson K, Persson M (2009) Beskrivning till jordartskartan 3 F Karlskrona NV & SV [Description of soil map 3 F Karlskrona NW & SW]. Sveriges Geologiska Undersökning K 155, SGU, Uppsala, Sweden, 11 pp
- Mendoza JA, Dahlin T, Barmen G (2006) Hydrogeological and hydrochemical features of an area polluted by heavy metals in central Nicaragua. *Hydrogeol J* 14:1052–1059
- Morris M, Rønning JS, Lile OB (1996) Geoelectric monitoring of a tracer injection experiment: modeling and interpretation. *Eur J Environ Eng Geophys* 1:15–34
- Neuendorf KKE, Mehl JP Jr, Jackson JA (2005) Glossary of Geology, 5th edn. American Geological Institute, Alexandria, VA
- Nilsson SI, Bergkvist B (1983) Aluminium chemistry and acidification processes in a shallow podzol on the Swedish west coast. *Water Air Soil Pollut* 20:311–330
- Nöjd P, Lindroos A-J, Smolander A, Derome J, Lumme I, Helmisaari H-S (2009) Artificial recharge of groundwater through sprinkling infiltration: impacts on forest soil and the nutrient status and growth of Scots pine. *Sci Total Environ* 407:3365–3371
- Okkonen J, Jyrkama M, Kløve B (2010) A conceptual approach for assessing the impact of climate change on groundwater and related surface waters in cold regions (Finland). *Hydrogeol J* 18:429–439
- Parsons ML (1970) Groundwater movement in a glacial complex, Cochrane district, Ontario. *Can J Earth Sci* 7(3):869–883
- Persson K (2008) Karlskrona vattenförsörjning, Utvärdering av spårämnesförsök i Johannishusåsen, etapp Västra Vång [Evaluation of tracer tests in Johannishus Ridge, West Vång stage]. SWECO 1240121000, Sweco, Malmö, Sweden, 8 pp
- Ringberg B (1969) Inventory of gravel deposits in the county. County Administrative Board of Blekinge, Karlskrona, Sweden, 314 pp
- Ringberg B (1976) Glacialgeologi och isavsmältning i östra Blekinge [Glacial geology and deglaciation in the eastern Blekinge]. SGU C661, Swedish Geological Survey, Uppsala, Sweden, 174 pp
- Russell AJ, Knudsen O, Fay H, Marren PM, Heinz J, Tronick J (2001) Morphology and sedimentology of a giant supraglacial, ice-walled, jökulhlaup channel, Skeidarárjökull, Iceland: implications for esker genesis. *Glob Planet Chang* 28:193–216
- SGU (2012) Digital geological and geophysical maps. Geol. Surv. of Sweden, Uppsala, Sweden
- Shreve RL (1985) Esker characteristics in terms of glacier physics, Katahdin esker system, Maine. *Geol Soc Am Bull* 96:639–646
- Singha K, Gorelick SM (2005) Saline tracer visualized with three-dimensional electrical resistivity tomography: field-scale spatial moment analysis. *Water Resour Res* 41(W05023):17
- Syverson KM, Gaffield SJ, Mickelson DM (1994) Comparison of esker morphology and sedimentology with former ice-surface topography, Burroughs Glacier, Alaska. *Geol Soc Am Bull* 106:1130–1142
- Thurman EM (1985) Humic substances in groundwater. In: Aiken GR, McKnight DM, Wershaw RL, MacCarthy P (eds) Humic substances in soil, sediment and water. Wiley, New York
- Warren WP, Ashley GM (1994) Origins of the ice-contact stratified ridges (eskers) of Ireland. *J Sediment Res* A64:433–449
- White PA (1988) Measurement of ground-water parameters using salt-water injection and surface resistivity. *Groundwater* 26:179–186
- White PA (1994) Electrode arrays for measuring groundwater flow direction and velocity. *Geophys* 59:192–201
- Yu S-Y (2003) The Littorina transgression in southeastern Sweden and its relation to mid-Holocene climate variability. PhD Thesis, Lundqua Thesis 51, Lund University, Sweden, 28 pp